Surface Science xxx (2015) xxx–xxx

Contents lists available at ScienceDirect

Surface Science

journal homepage: www.elsevier.com/locate/susc

Promotion of CO oxidation on PdO(101) by adsorbed H_2O

Juhee Choi [a], Li Pan [b], Vikram Mehar [a], Feng Zhang [a], Aravind Asthagiri [b], Jason F. Weaver [a,*]

[a] Department of Chemical Engineering, University of Florida, Gainesville, FL 32611, USA
[b] William G. Lowrie Chemical & Biomolecular Engineering, The Ohio State University, Columbus, OH 43210, USA

ARTICLE INFO

Available online xxxx

Keywords:
CO oxidation
PdO
Pd
Water adsorption
DFT
RAIRS

ABSTRACT

We investigated the influence of adsorbed H_2O on the oxidation of CO on PdO(101) using temperature programmed reaction spectroscopy (TPRS), reflection absorption infrared spectroscopy (RAIRS) and density functional theory (DFT) calculations. We find that water inhibits CO adsorption on PdO(101) by site blocking, but also provides a more facile pathway for CO oxidation compared with the bare oxide surface. In the presence of adsorbed H_2O, the oxidation of CO on PdO(101) produces a CO_2 TPRS peak that is centered at a temperature ~50 K lower than the main CO_2 TPRS peak arising from CO oxidation on clean PdO(101) (~330 vs. 380 K). RAIRS shows that CO continues to adsorb on atop-Pd sites of PdO(101) when H_2O is co-adsorbed, and provides no evidence of other reactive intermediates. DFT calculations predict that the CO oxidation mechanism follows the same steps for CO adsorbed on PdO(101) with and without co-adsorbed H_2O, wherein an atop-CO species recombines with an oxygen atom from the oxide surface lattice. According to DFT, hydrogen bonding interactions with adsorbed H_2O species stabilize the carboxyl-like transition structure and intermediate that result from the initial recombination of CO and O on the PdO(101) surface. This stabilization lowers the energy barrier for CO oxidation on PdO(101) by ~10 kJ/mol, in good agreement with our experimental estimate.

1. Introduction

The oxidation of CO on late transition metals is important in many energy and environmental applications and has served as a prototypical reaction for uncovering fundamental principles in gas-surface interactions. Investigations using in situ surface diagnostics have shown that the CO oxidation activity of late transition-metals tends to increase significantly near the onset of metal oxide formation [1–4]. Consistent with these reports, prior studies show that crystalline RuO_2(110) and PdO(101) surfaces are highly active toward CO oxidation under ultra-high vacuum (UHV) conditions [5,6]. Water is present in many catalytic applications, and can influence CO oxidation in multiple ways. In general, adsorbed water has been found to enhance the oxidation of CO on oxygen-covered metal surfaces, including Pt, Pd and Au surfaces [7–12]. For example, Ojifinni et al. [8] report that exposing O-covered Au(111) to water enhances CO oxidation rates and present evidence that direct reactions between co-adsorbed CO and OH groups are responsible for the improved reactivity. DFT calculations predict that a similar mechanism can explain the promotional effects of water on the oxidation of CO on other close-packed metal surfaces [11,12].

In contrast to the behavior reported for metal surfaces, several investigations report that water poisons the CO oxidation activity of various transition-metal oxides, including Co_3O_4, MnO and CuO [12–17]. DFT calculations predict that the poisoning effect on Co_3O_4 and possibly other metal oxides results from a lower reactivity of OH groups, which form by reaction between H_2O and lattice oxygen, compared with the lattice oxygen itself [12]. This prediction suggests that the influence of water on CO oxidation may depend, in part, on the tendency of H_2O to deprotonate on the particular metal oxide surface. Of particular relevance to the present study is a report by Oh and Hoflund showing that CO oxidation is more facile on hydrous PdO powders compared with anhydrous PdO [18]. Those authors suggest that reaction with surface OH groups is responsible for the higher catalytic activity of hydrous PdO, contrary to the DFT predictions mentioned above. These prior investigations signal a need for further study of the effects of water on CO oxidation over transition metal oxides, particularly experimental work using oxide surfaces with well-defined structure.

We have previously investigated CO adsorption and oxidation as well as water adsorption on a crystalline PdO(101) thin film [19–23]. We find that the oxidation of CO is facile on PdO(101) as more than 70% of the CO molecules in a saturated layer are oxidized to CO_2 during temperature programmed reaction spectroscopy (TPRS) via reaction with the oxide surface [21]. The oxidation of CO on PdO(101) gives rise to two main CO_2 TPRS peaks at ~380 and 530 K that originate from the oxidation of CO molecules that are adsorbed on coordinatively unsaturated (cus) Pd sites located next to surface O-atoms vs. next to surface oxygen vacancies, respectively. Our results demonstrate that a strong enhancement in the binding energy causes CO molecules to rapidly diffuse to Pd_{cus} sites that are located next to oxygen vacancies as such sites are created during TPRS. We have also reported that water adsorbs strongly on the Pd_{cus} sites of PdO(101). We find that the formation

* Corresponding author. Tel.: +1 352 392 0869; fax: +1 352 392 9513.
E-mail address: weaver@che.ufl.edu (J.F. Weaver).

http://dx.doi.org/10.1016/j.susc.2015.08.043
0039-6028/

of HO–H_2O complexes along the Pd_{cus} rows is preferable for water coverages up to 50% of the Pd_{cus} site density, and that molecular adsorption of H_2O commences thereafter [19]. The desorption of chemisorbed water from PdO(101) and CO oxidation occur over a similar range of temperatures (~325 to 400 K), suggesting that H_2O–CO interactions may influence the CO oxidation kinetics.

In the present study, we show that adsorbed water provides a more facile pathway for CO oxidation on PdO(101) compared with reaction on the clean oxide surface. DFT calculations predict that this promotional effect arises from hydrogen-bonding interactions between molecular H_2O and the carboxyl-like transition structure for CO oxidation on PdO(101).

2. Experimental details

The experiments reported in this study were conducted in an ultrahigh vacuum (UHV) chamber with a typical base pressure of 5×10^{-11} Torr [21,23]. The Pd(111) crystal used in the present study is a circular disk (8 mm × 1 mm) spot-welded to W wires and attached to a copper sample holder that is in thermal contact with a liquid nitrogen cooled reservoir. A type K thermocouple is spot-welded to the backside of the crystal to measure the sample temperature. The sample is resistively heated and the temperature is controlled using a PID controller that adjusts the output of a dc power supply. In this setup, we are able to maintain or linearly ramp the sample temperature from 85 to 1250 K. Initial sample cleaning consisted of cycles of sputtering with 600 eV Ar^+ ions at a surface temperature of 900 K, followed by annealing at 1100 K for 5 min. Subsequent cleaning involved routinely exposing the sample to an atomic oxygen beam for 30 min at 850 K, followed by flashing the sample to 923 K to desorb oxygen and carbon oxides. As discussed previously [24], we limited the sample temperature to 923 K to maintain saturation of oxygen in the subsurface reservoir, which ensures reproducibility in preparing the PdO(101) thin films. We considered the Pd(111) sample to be clean when we could not detect contaminants with Auger electron spectroscopy (AES) and did not observe CO production during temperature-programmed desorption after oxygen adsorption.

We generate a PdO (101) thin film by exposing the Pd(111) surface to an ~23 ML dose of oxygen atoms at 500 K, followed by briefly heating to 600 K, where we define 1 ML as equal to the Pd(111) surface atom density of 1.53×10^{15} cm^{-2}. This procedure generates a PdO(101) surface with identical surface structure and chemical properties to those studied previously [25–27]. We provide details of the PdO(101) surface structure in the Computational details section. We used temperature programmed reaction spectroscopy (TPRS) to investigate CO oxidation on the PdO(101) film with and without pre-adsorbed water. We used deionized water in our experiments and further purified the water using several freeze–pump–thaw cycles prior to admission into the UHV chamber. To generate co-adsorbed CO + H_2O layers, we first adsorbed H_2O on the PdO(101) surface at 90 K, followed by flashing to 275 K, and subsequently exposed the water pre-covered surface to CO at 90 K. Heating the water-exposed surface to 275 K causes water adsorbed in the multilayer and on Pd_{4f} sites to desorb [19], and possibly redistribute, thereby generating a surface in which H_2O and OH species bind only to the Pd_{cus} sites.

We collected TPRS spectra by positioning the PdO(101) surface in front of a shielded quadrupole mass spectrometer (Hiden) at a distance of ~5 mm. The sample temperature increases to 700 K at 1 K/s as the mass spectrometer monitors H_2O, CO and CO_2 desorption from the surface. The CO desorption yield measured in the TPRS spectrum is estimated by scaling CO TPD spectra obtained after saturating Pd(111) with CO at 200 K, assuming that the saturation coverage is 0.66 ML [28]. The CO_2 yield is estimated by assuming that the saturated CO layer on PdO(101) at 95 K generates 0.24 ML of CO_2 as reported previously [21]. We estimated H_2O coverages by scaling integrated TPD spectra collected from an H_2O monolayer prepared on PdO(101) at 90 K, assuming a saturation coverage of 0.70 ML [19]. All RAIR spectra reported in this study were collected at a sample temperature of 90 K and each spectrum is an average of 512 scans.

3. Computational details

The periodic plane wave DFT calculations reported in this paper were performed using the Vienna ab initio simulation package (VASP) [29,30] with projector augmented wave (PAW) [31] pseudopotentials provided in the VASP database. The Perdew–Burke–Ernzerhof (PBE) exchange–correlation functional [32] was used with a plane wave cutoff of 400 eV. Fig. 1 illustrates the stoichiometric PdO(101) surface that is investigated in this study. Bulk crystalline PdO has a tetragonal unit cell and consists of square planar units of Pd atoms fourfold coordinated with oxygen atoms. The bulk-terminated PdO(101) surface is defined by a rectangular unit cell, where the *a* and *b* lattice vectors coincide with the [010]and $[\bar{1}01]$ directions of the PdO crystal, respectively. The stoichiometric PdO(101) surface consists of alternating rows of threefold or fourfold coordinated Pd or O atoms that run parallel to the *a* direction shown in Fig. 1. Thus, half of the surface O and Pd atoms are coordinatively unsaturated (cus). The areal density of each type of coordinatively-distinct atom of the PdO(101) surface is equal to 35% of the atomic density of the Pd(111) surface. Hence, the coverage of cus-Pd atoms is equal to 0.35 ML, and each PdO(101) layer contains 0.7 ML of Pd atoms and 0.7 ML of O atoms.

The PdO(101) surface was modeled by a rectangular 4 × 1 unit cell, with a corresponding 4 × 2 × 1 Monkhorst–Pack k-point mesh [21]. As in our prior studies [33–35], the PdO(101) film was strained (a = 3.057 Å, b = 6.352 Å) to match the PdO(101) film structure resolved by Kan and Weaver [25,26]. The PdO(101) slab was represented by four layers resulting in a 9 Å thick slab. The bottom layer is fixed, but other lattice atoms are allowed to relax until the forces are less than 0.03 eV/Å. As in our previous work, the underlying Pd(111) surface is not included since this would require a large unit cell due to the registry of the PdO(101) film with the Pd(111) surface. We use a vacuum spacing of 20 Å, which is sufficient to eliminate spurious interactions in the surface normal direction. We determined the barriers and pathway for CO_2 formation on the PdO(101) surface using the climbing nudged elastic band (cNEB) method [36]. Vibrational frequencies were calculated

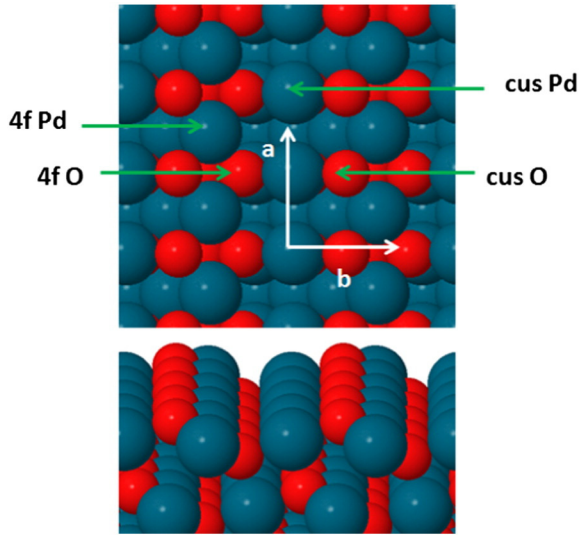

Fig. 1. Top and side views of the PdO(101) surface. The red and dark blue atoms represent O and Pd atoms, respectively. Rows of coordinatively unsaturated (cus) and fourfold-coordinated (4f) Pd or O atoms are indicated. The vertical and horizontal arrows a and b represent the [010]and $[\bar{1}01]$ crystallographic directions of PdO. (For interpretation of the references to color in this figure legend, the reader is referred to the web version of this article.)

Please cite this article as: J. Choi, et al., Surf. Sci. (2015), http://dx.doi.org/10.1016/j.susc.2015.08.043

with only the degrees of freedom associated with the CO and water molecules included. We performed calculations for selected configurations and find that including the motions of the neighboring Pd and O atoms in the normal mode analysis has a negligible effect (<2 cm^{-1}) on the computed C—O stretch frequencies. The obtained frequencies were corrected by scaling with a factor of 1.024, which is the ratio of the experimental harmonic gas phase C—O stretch frequency (~2170 cm^{-1}) and the corresponding calculated value (~2120 cm^{-1}) in PBE. This approach to scale the DFT vibrational frequency has been shown to give good agreement with experimental RAIRS data [23]. Finally, we define the CO adsorption (or binding) energy as follows $E_{ads} = {}^{-(E_{CO/surf}-(NE_{CO}+E_{surf}))}/_{N}$, where E_{CO} is the energy of an isolated CO molecule and $E_{CO/surf}$ and E_{surf} are the energy of surface slab with N CO molecules and water co-adsorbed and the surface slab with pre-adsorbed water, respectively.

In a previous study of CO oxidation on PdO(101) [21], we found that PBE-DFT overestimates the binding energy of CO adsorbed on bridge-Pd_{cus} sites, resulting in similar adsorption energies for CO adsorbed on the atop and bridge Pd_{cus} sites. RAIRS spectra indicate that CO adsorbs only on the atop Pd_{cus} sites of PdO(101) and DFT calculations performed with the Heyd–Scuseria–Ernzerhof (HSE) functional confirm this observation [21]. Because of the difficulty of performing fully relaxed HSE-DFT calculations, we have only tested the adsorption energy of CO adsorbed on the atop and bridge Pd_{cus} site next to a single water molecule using static HSE calculations. We confirmed that HSE-DFT predicts that the atop site is still favored over the bridge Pd_{cus} site by ~50 kJ/mol in the presence of H_2O. We thus constrain our computations to study the adsorption and oxidation of CO bound on the atop Pd_{cus} site, which has been successfully used in our previous studies of CO oxidation on a bare PdO(101) surface [20–22].

4. Results and discussion

Fig. 2 shows CO_2 and CO TPRS traces obtained as a function of the initial CO coverage prepared on PdO(101) at 90 K. The CO_2 TPRS spectra exhibit two distinct maxima at 380 and 530 K (χ_2 and χ_1) which grow concurrently as the initial CO coverage increases. We have recently reported CO_2 and CO TPRS data obtained from a saturated CO layer on PdO(101) generated at 90 K [21]. This prior study shows that CO molecules adsorb exclusively on atop-Pd_{cus} sites of PdO(101), and that the low and high temperature CO_2 features originate from the oxidation of atop-CO molecules adsorbed next to O_{cus} atoms vs. next to O_{cus} vacancies, which we designate as CO–Pd_{cus}/O_{cus} and CO–Pd_{cus}/O_v species, respectively [20,21]. We estimate that CO reaches a saturation coverage of 0.34 ML on PdO(101), which is nearly equal to the Pd_{cus} site density (0.35 ML), and that 72% of the adsorbed CO is oxidized to CO_2 during TPRS when the CO layer is initially saturated.

The data shown in Fig. 2 demonstrates that the fractional CO_2 yield is essentially invariant with increasing CO coverage, with values ranging from 72% and 80%. In general, a kinetic competition between CO desorption vs. reaction with O_{cus} atoms determines the CO_2 product yield, with the high yields that are observed indicating that the kinetic branching favors CO reaction over desorption during TPRS [21]. The shapes of the CO_2 TPRS traces are also relatively insensitive to the CO coverage—the relative intensities of the χ_2 and χ_1 CO_2 peaks remain nearly constant with increasing CO coverage, and the same CO_2 features are dominant at the CO coverages studied. These characteristics suggest that oxidation of the CO–Pd_{cus}/O_{cus} and CO–Pd_{cus}/O_v species is the predominant reaction pathway at all CO coverages and that the initial CO coverage has little effect on the reaction kinetics. The CO TPD traces also exhibit two main peaks (388 K and 550 K) that arise from CO desorbing from Pd_{cus}/O_{cus} and Pd_{cus}/O_v sites, respectively. The CO TPD features observed below about 200 K are consistent with CO desorption from the sample support structure and are omitted from our quantitative analysis.

TPRS experiments reveal that adsorbed water provides a low-temperature pathway for the oxidation of CO on the PdO(101) surface. Fig. 3 compares CO_2 and H_2O TPRS traces obtained from a pure CO layer with 0.15 ML initial CO coverage, and from a mixed CO + H_2O layer with initial coverages of 0.13 ML of CO and 0.10 ML of H_2O. The CO_2 yield is ~0.11 ML in both experiments. The CO_2 TPRS trace obtained from the mixed layer exhibits a predominant peak at ~327 K, while the peak at 380 K is significantly less intense compared with that obtained from the pure CO layer. Since the initial CO coverage is nearly the same in each experiment, the appearance of the 327 K CO_2 peak (χ_3) and the concurrent diminution of the 380 K CO_2 peak (χ_2) show that pre-adsorbed H_2O promotes the oxidation of a large fraction of the CO molecules adsorbed on PdO(101). Assuming a pre-factor of 10^{12} s^{-1}, the Redhead equation predicts activation energies of 82.1 and 95.3 kJ/mol for CO_2 desorption in the χ_3 and χ_2 peaks, respectively, which gives a difference of about 13 kJ/mol between these reaction barriers. Notice also that the χ_3 CO_2 peak maximum lies below the H_2O peak maximum (~327 vs. 340 K), thus demonstrating that H_2O is adsorbed on the surface when CO_2 evolves in the χ_3 TPRS peak.

Fig. 4a shows a series of CO_2 TPRS spectra obtained from mixed layers of CO and H_2O on PdO(101) as a function of the pre-adsorbed H_2O coverage. The layers were prepared by adsorbing H_2O to a specific coverage, followed by a saturation exposure of CO at 90 K. Under these conditions, we find that the initial H_2O + CO coverage is close to the Pd_{cus} site density, with values ranging from 0.32 to 0.34 ML. The CO_2

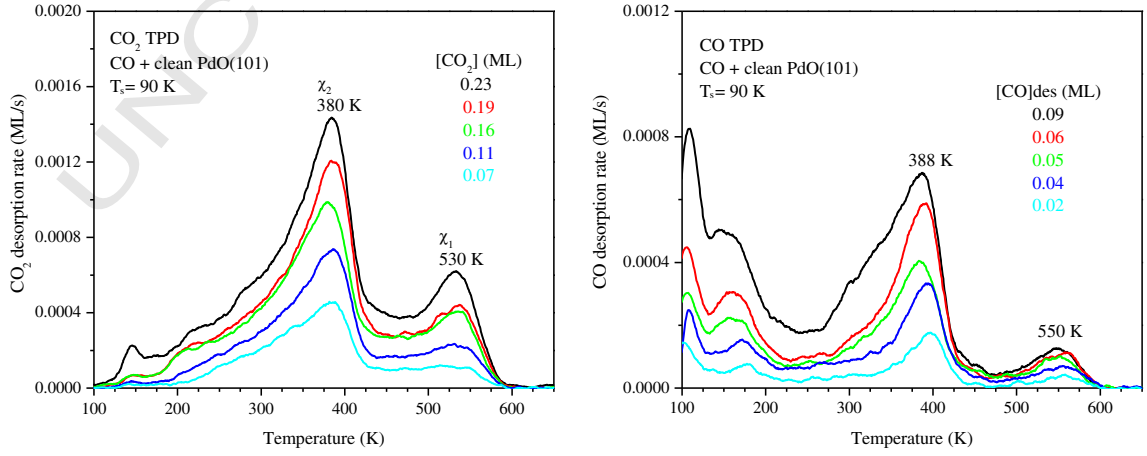

Fig. 2. (a) CO_2 and (b) CO TPRS traces obtained after preparing different initial coverages of CO on clean PdO(101) at 90 K.

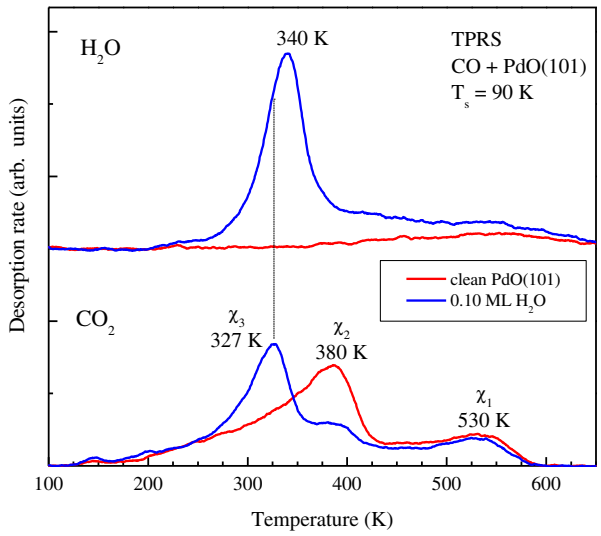

Fig. 3. H_2O (top) and CO_2 (bottom) TPRS traces obtained after adsorbing 0.15 ML of CO on clean PdO(101) (red) vs. 0.13 ML of CO on PdO(101) covered with 0.10 ML of pre-adsorbed H_2O (blue). (For interpretation of the references to color in this figure legend, the reader is referred to the web version of this article.)

TPRS traces exhibit two main changes as a function of the initial water coverage. First, the total CO_2 yield decreases with increasing H_2O coverage due to water blocking CO adsorption sites. Also, the intensity of the χ_3 CO_2 peak increases relative to the higher temperature χ_2 and χ_1 TPRS peaks as the water pre-coverage increases.

Fig. 4b shows how the initial H_2O coverage influences the CO_2 desorption yields and selectivity toward the low temperature, water-assisted pathway. The quantitative analysis reveals that the total CO_2 yield decreases linearly with increasing H_2O coverage. In fact, assuming that each H_2O molecule occupies a single Pd_{cus} site, we find that the initial CO coverage increases linearly with the coverage of empty Pd_{cus} sites. Prior studies show that both H_2O and CO molecules preferentially adsorb on atop-Pd_{cus} sites, and that each molecule occupies a single Pd_{cus} site [19,21]. The behavior that we observe here demonstrates that pre-adsorbed H_2O is highly effective in preventing CO from adsorbing on Pd_{cus} sites (i.e., CO negligibly displaces H_2O under the conditions studied), and shows that CO can adsorb in close proximity to pre-adsorbed H_2O. The latter conclusion is reached by recognizing that total H_2O + CO coverages greater than 90% of the Pd_{cus} site density were generated in each experiment.

Although adsorbed H_2O blocks CO adsorption sites, we find that the fraction of CO_2 which desorbs below 360 K increases with increasing water pre-coverage, with values increasing from 42% to 68% for H_2O coverages up to 0.24 ML (Fig. 4b). Thus, the branching toward the low temperature pathway increases with increasing water coverage. Interestingly, our analysis shows that a considerable fraction of CO reacts via the higher temperature χ_2 and χ_1 channels even when H_2O is adsorbed in larger quantities than CO. Since water desorbs nearly concurrently with CO_2 evolution in the χ_3 peak (Fig. 3), a possibility is that H_2O desorption limits the amount of CO that reacts by the water-assisted pathway during TPRS. We also find that the yield of CO_2 which desorbs below 360 K remains largely invariant with increasing H_2O coverage to about 0.10 ML, and decreases with increasing H_2O coverage thereafter (Fig. 4b). A water pre-coverage of 0.10 ML appears to represent an optimum wherein low temperature CO oxidation occurs with both high yield and high selectivity.

Our TPRS results suggest that the water-assisted pathway does not involve oxygen exchange between H_2O and CO. For example, for a given initial H_2O coverage, we find that the H_2O desorption yield is the same in TPRS experiments performed with varying coverages of CO, even though the yield of CO_2 evolving in the χ_3 peak increases with increasing CO coverage. The DFT calculations discussed below also predict that the promotional effect results from H_2O stabilization of the transition state to CO_2 rather than interatomic exchange between the CO and H_2O adsorbates. Although we have not performed experiments using co-adsorbed $H_2^{18}O$ and CO, we believe that our results support the conclusion that H_2O does not provide oxygen to CO during the TPRS experiments.

Fig. 5 compares RAIR spectra obtained after adsorbing 0.15 ML of CO on clean PdO(101) vs. preparing a mixture of 0.13 ML of CO and 0.10 ML of pre-adsorbed H_2O, and heating to the specified temperatures. The RAIR spectrum obtained from the pure CO layer exhibits a single C—O stretch band at 2146 cm^{-1} that arises from atop-CO adsorbed on Pd_{cus}/O_{cus} sites. The RAIR spectrum obtained from the mixed layer at 90 K also exhibits only a single C—O stretch band that is redshifted by

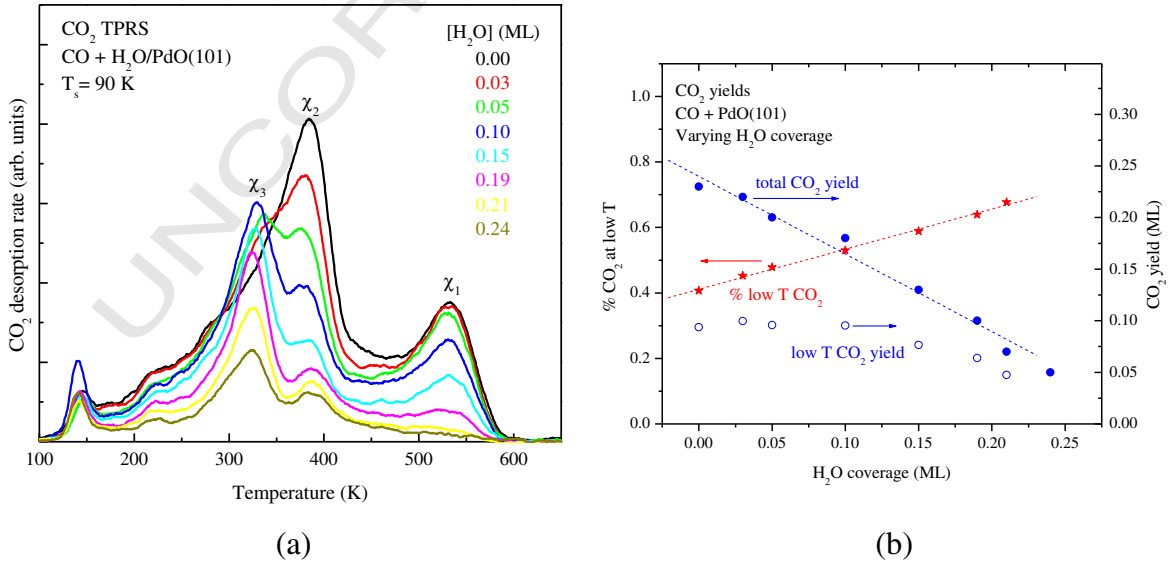

Fig. 4. (a) CO_2 TPRS traces obtained as a function of the H_2O pre-coverage on PdO(101) that was exposed to saturation doses of CO at 90 K. In each experiment, the total, initial coverage of H_2O + CO was between 0.32 and 0.34 ML. (b) Total and low-temperature (<360 K) CO_2 yields (solid blue and open blue symbols) and the fractional yield of low-temperature CO_2 (red symbols) obtained during TPRS as a function of the H_2O pre-coverage on PdO(101). The dashed lines are linear fits to the data. (For interpretation of the references to color in this figure legend, the reader is referred to the web version of this article.)

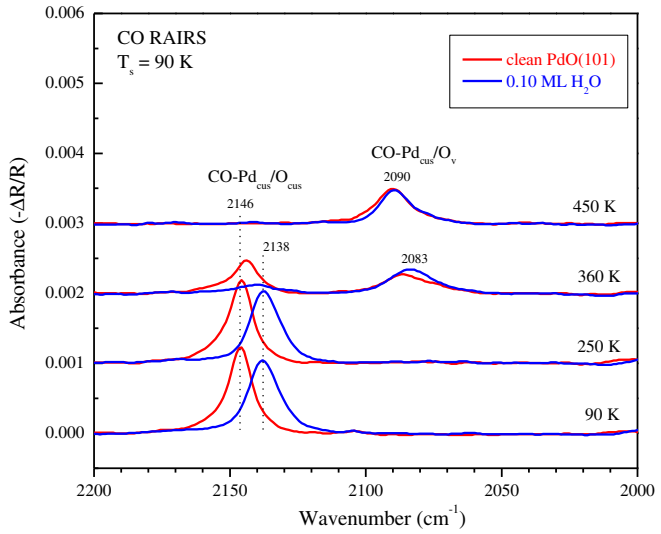

Fig. 5. Heating series of RAIR spectra obtained from 0.15 ML of CO initially adsorbed on PdO(101) at 90 K (red) vs. 0.13 ML of CO initially adsorbed on PdO(101) with 0.10 ML of pre-adsorbed H_2O (blue). (For interpretation of the references to color in this figure legend, the reader is referred to the web version of this article.)

about 8 cm^{-1} relative to that obtained from the pure CO layer on PdO(101). The appearance of a single feature at 2138 cm^{-1} and the lack of other RAIRS peaks provides strong evidence that CO and H_2O do not react to produce distinct compounds on PdO(101) under the conditions studied, and that CO continues to adsorb on atop-Pd_{cus} sites when H_2O is pre-adsorbed. Although relatively small, the redshift demonstrates that an interaction between co-adsorbed CO and H_2O on PdO(101) slightly softens the C—O bond of the CO–Pd_{cus}/O_{cus} species. We find that the C—O stretch band redshifts only slightly with increasing CO coverage in both the pure and mixed layers on PdO(101), with values ranging from 2147 to 2144 cm^{-1} for the pure CO layer and from 2140 to 2138 cm^{-1} when 0.10 ML H_2O is initially adsorbed, respectively. The RAIR spectra change negligibly after heating the layers to 250 K.

After heating to 360 K, the RAIR spectrum obtained from the pure CO layer exhibits two peaks at 2143 and 2083 cm^{-1}, where the latter corresponds to the CO–Pd_{cus}/O_v species [20–22]. The peak at 2143 cm^{-1} is less intense compared with that observed in the initial spectrum obtained from the CO layer because a fraction of the CO–Pd_{cus}/O_{cus} species desorb, react and move to Pd_{cus}/O_v sites. Heating to 360 K causes the C—O stretch peak near 2138 cm^{-1} to diminish to a greater extent for the mixed layer relative to the pure CO layer. This difference is consistent with the larger amount of CO_2 produced below 360 K in the mixed vs. the pure CO layers (Fig. 3), and thus a larger decrease in the concentration of CO–Pd_{cus}/O_{cus} species in the mixed layer. The peaks at 2083 cm^{-1} are similar in intensity after heating the pure and mixed layers to 360 K, suggesting that adsorbed H_2O negligibly affects the diffusion of CO to Pd_{cus}/O_v sites. Finally, after heating to 450 K, the RAIRS peak near 2140 cm^{-1} is no longer visible and the spectra obtained from both layers exhibit a feature at 2090 cm^{-1} of nearly the same intensity, indicating that similar quantities of CO–Pd_{cus}/O_v species form on each surface as the layers are heated beyond the temperatures at which the CO–Pd_{cus}/O_{cus} species oxidize. The similar yields of the χ_1 CO_2 TPRS peaks observed at 530 K for the pure and mixed CO layers (Fig. 3) support the conclusion that similar concentrations of CO–Pd_{cus}/O_v species are generated on these surfaces.

4.1. Computational results

We performed DFT calculations to investigate the adsorption and oxidation of CO on PdO(101) with co-adsorbed water, aiming to determine the mechanism for the water-assisted pathway for CO oxidation. We have previously reported that H_2O prefers to form a hydrogen-bonded HO–H_2O complex on PdO(101), in which the H_2O molecule acts as the hydrogen donor and each adsorbate binds to a Pd_{cus} atom [19]. The HO–H_2O complex is energetically favored over isolated H_2O molecules on PdO(101) by ~40 kJ/mol and is favored over an adsorbed H_2O–H_2O dimer by 28 kJ/mol. Fig. 6 shows models of the CO + H_2O configurations that we investigated and Table 1 lists the corresponding CO binding energies and C—O stretch frequencies computed using DFT. The CO binding energies represent the energy required to remove a CO molecule from each of the adsorbed H_2O configurations shown.

DFT calculations predict that pre-adsorbed H_2O lowers the CO binding energy on PdO(101) but that the decrease in stability is relatively insensitive to the initial water configuration when the CO molecule has only one H_2O or OH neighbor on the Pd_{cus} row. For example, we predict a binding energy of 133 kJ/mol for CO to adsorb next to a single H_2O molecule on PdO(101), compared with 141 kJ/mol for CO adsorption on clean PdO(101). The CO binding energy lies between 131 and 134 kJ/mol for CO adsorption onto the other water configurations studied (Table 1).

Compared with the binding energy, the C—O stretch frequency in the various CO + H_2O/OH mixtures is more sensitive to the local environment and is predicted to red-shift relative to the C—O stretch frequency of CO adsorbed on clean PdO(101). We predict the largest red-shifts (40 to 45 cm^{-1}) for CO adsorbed next to a single H_2O molecule or a H_2O–H_2O dimer, whereas the red-shifts lie between 13 and 20 cm^{-1} for CO adsorbed next to the HO–H_2O complex on PdO(101). The smaller red-shifts of the C—O stretch band predicted for the CO + HO–H_2O complex configurations are more consistent with the shift of ~8 cm^{-1} that we observe for the CO + H_2O mixed layer using RAIRS (Fig. 5). Considering the favorable stability of the HO–H_2O complex relative to other H_2O/OH configurations, we conclude that the measured red-shift of the C—O stretch band arises mainly from CO molecules adsorbed in close proximity to HO–H_2O complexes on PdO(101).

DFT calculations predict that adsorbed H_2O molecules can stabilize the transition state for CO oxidation and thereby lower the energy

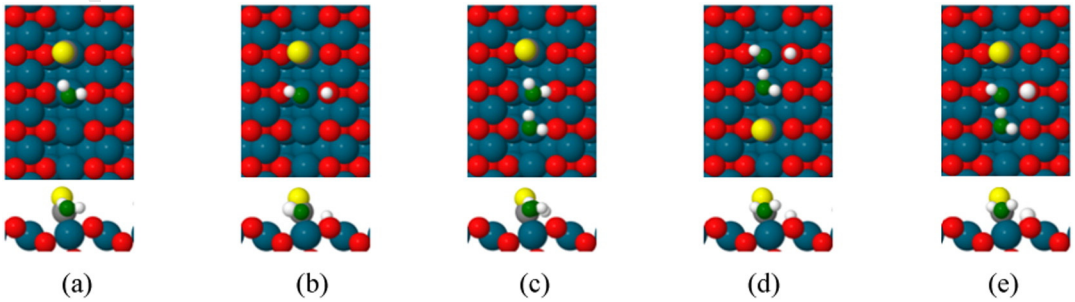

Fig. 6. Top and side views of CO + H_2O configurations investigated using DFT: a) 25% H_2O + 25% CO, b) 25% HO–HO_{cus} + 25% CO, c) 50% H_2O + 25% CO (CO–H_2O–H_2O), d) 50% HO–H_2O complex + 25% CO (CO–H_2O end), and e) 50% HO–H_2O complex + 25% CO (CO–HO–HO_{cus} end). Green and white spheres denote the O and H atoms in water. Yellow and grey spheres denote the O and C atoms in CO. (For interpretation of the references to color in this figure legend, the reader is referred to the web version of this article.)

Please cite this article as: J. Choi, et al., Surf. Sci. (2015), http://dx.doi.org/10.1016/j.susc.2015.08.043

Table 1
Calculated adsorption energy (E_{ad}) per CO molecule and stretch frequencies (ν) of CO in different CO + H_2O configurations (see Fig. 6).

	Configuration	E_{ad}/(kJ/mol)	ν (cm^{-1})
Ref	25% CO	141	2136
A	25% H_2O + 25% CO	133	2097
B	25% HO–HO_{cus} + 25% CO	134	2132
C	50% H_2O + 25% CO (CO–H_2O–H_2O)	131	2092
D	50% HO–H_2O complex + 25% CO (H_2O end)	133	2123
E	50% HO–H_2O complex + 25% CO (OH end)	131	2116

barrier for reaction. The stabilization mechanism relies on the ability of adsorbed H_2O molecules to hydrogen-bond with the carboxyl-like transition structure, and occurs only for certain H_2O configurations. Notably, Gong et al. predict that a similar stabilizing interaction can lower the CO oxidation barrier in mixed CO + H_2O layers on metal surfaces as well [11]. We predict that the HO–H_2O complex (either at the H_2O or HO–HO_{cus} end) has a negligible promotional effect on the CO oxidation reaction on PdO(101), in that the energy barrier (63 kJ/mol) and reaction pathway is the same when CO is adsorbed on clean PdO(101) vs. next to the HO–H_2O complex. For CO adsorbed next to an isolated H_2O molecule or a H_2O–H_2O dimer, we predict that the energy barrier for CO oxidation is lower by about 10 kJ/mol compared with that on the clean PdO(101) surface, in good agreement with the energy difference estimated from our TPRS data.

Fig. 7a and b show energy diagrams for the oxidation of CO adsorbed next to a HO–H_2O complex and next to a H_2O–H_2O dimer, respectively. For both pathways, the adsorbed CO molecule first abstracts the neighboring O_{cus} atom to produce a carboxyl ($CO_2^{\delta-}$) intermediate, and the intermediate subsequently transforms to CO_2 which desorbs and leaves an O_v site on the surface. The key difference between these reaction pathways is the stabilizing interaction that occurs between the carboxyl transition structure (and intermediate) and the H_2O molecule of the H_2O–H_2O dimer, and the lack of such an interaction for CO oxidation next to the HO–H_2O complex. The molecular images of the CO_2—H_2O–H_2O transition structure and intermediate show that the nearby H-atom of H_2O and an O-atom of the carboxyl species lie in close proximity, at a distance that is consistent with a hydrogen-

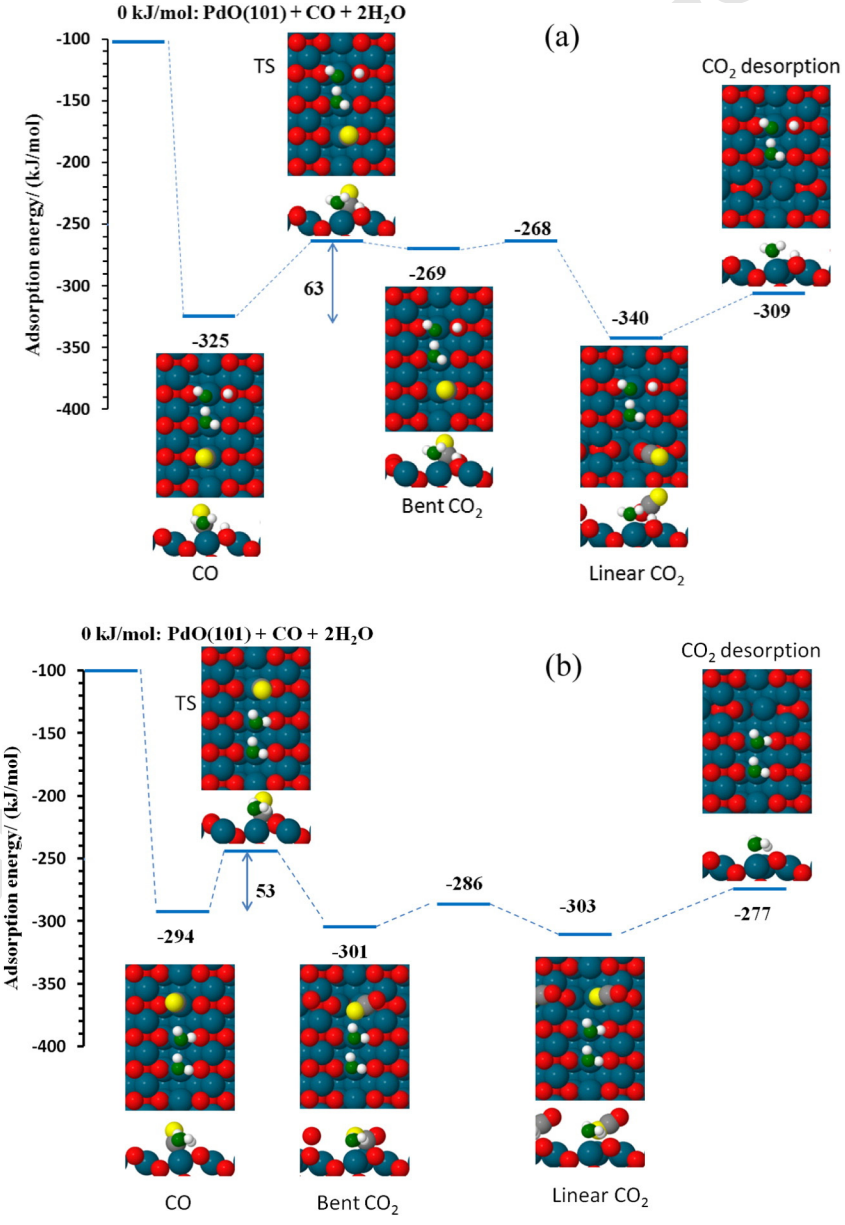

Fig. 7. Energy diagrams for the oxidation of CO adsorbed (a) next to a HO–H_2O complex and (b) next to a H_2O–H_2O dimer.

Please cite this article as: J. Choi, et al., Surf. Sci. (2015), http://dx.doi.org/10.1016/j.susc.2015.08.043

bonding interaction. The formation of a hydrogen bond is particularly evident in the image of the carboxyl intermediate as one may notice that the $CO_2^{\delta-}$ moiety is rotated toward the H_2O molecule to enable the hydrogen-bonding interaction (Fig. 7b).

In contrast, the HO–H_2O complex is relatively distant from the carboxyl transition structure and intermediate, and the position of the complex remains essentially unchanged as the neighboring CO molecule reacts with an O_{cus} atom. The weak interaction between CO_2 and the HO–H_2O complex may be understood by considering the nature of the HO–H_2O interaction. First, the OH species of the complex is slightly anionic [19] and thus interacts unfavorably with an O-atom of the $CO_2^{\delta-}$ transition structure. Also, when CO is adsorbed next to the H_2O molecule of the HO–H_2O complex, the H_2O molecule does not adjust its position to interact with the CO_2 transition structure, likely because such a rearrangement would weaken the strong HO–H_2O hydrogen bond.

The reaction energetics further demonstrate the stabilization afforded by hydrogen-bonding between the carboxyl and H_2O species. For the CO–HO–H_2O configuration, hydrogen bonding provides negligible stabilization of the carboxyl transition state, and DFT predicts that $CO_2^{\delta-}$ formation is endothermic by 56 kJ/mol, with an energy barrier of 63 kJ/mol (Fig. 7a). For the CO–H_2O–H_2O structure, DFT predicts that $CO_2^{\delta-}$ formation is actually exothermic by 7 kJ/mol and that the corresponding barrier is 53 kJ/mol (Fig. 7b). Thus, according to DFT, hydrogen bonding with H_2O stabilizes the $CO_2^{\delta-}$ intermediate by about 63 kJ/mol, and lowers the barrier for CO + O_{cus} recombination by 10 kJ/mol. The subsequent transformation of the $CO_2^{\delta-}$ species to CO_2 as well as the desorption of CO_2 should occur readily for both configurations because the energy barriers for these steps are considerably smaller than the barrier for initial $CO_2^{\delta-}$ formation.

Overall, the picture that emerges from our experiments and DFT calculations is that the mixed CO + H_2O layers prepared at 90 K consist mainly of CO and HO–H_2O complexes that interact only weakly with one another, but that the complexes decompose during heating and produce H_2O molecules that stabilize the transition structure for CO oxidation and thereby afford a low-energy pathway for CO oxidation. Recall that the water-assisted CO oxidation process occurs over a similar range of temperature as the desorption of H_2O from mixed CO + H_2O layers on PdO(101) (Fig. 3). As such, it is reasonable to assert that meta-stable H_2O molecules are responsible for stabilizing the CO_2 transition state since the HO–H_2O complexes necessarily undergo protonation via adjacent HO_{cus} groups and decomposition into H_2O monomers prior to desorption [19]. Furthermore, the energy required for the HO–H_2O complexes to transform to isolated H_2O molecules is less than the energy barrier for CO oxidation via the water-assisted pathway (~30 vs. 53 kJ/mol). Thus, the populations of H_2O monomers and dimers are likely to be high at the temperatures at which water-assisted CO oxidation occurs at appreciable rates, and would thus be available in sufficient quantities to promote CO oxidation.

5. Summary

We used TPRS, RAIRS and DFT calculations to investigate the effects of adsorbed H_2O on the oxidation of CO on PdO(101). We find that water inhibits the adsorption of CO by blocking Pd_{cus} sites, but also provides a facile pathway for CO oxidation on PdO(101). The oxidation of CO in co-adsorbed CO + H_2O layers on PdO(101) produces a CO_2 TPRS peak that is centered at a temperature ~50 K lower than the CO_2 TPRS peak resulting from CO oxidation on pristine PdO(101) (~330 vs. 380 K). The relative yield of CO_2 that evolves below 360 K increases linearly with increasing H_2O coverage up to at least 75% of the Pd_{cus} site density. According to DFT, H_2O monomers and dimers stabilize the carboxyl-like transition structure via hydrogen bonding, and thereby lower the barrier for CO oxidation on PdO(101) by ~10 kJ/mol, in good agreement with our experimental estimate. The DFT calculations predict that the stable HO–H_2O complex on PdO(101) has a negligible influence on the energetics for CO oxidation, and thus suggest that the water-assisted reaction pathway involves adsorbed H_2O species that are meta-stable relative to the preferred HO–H_2O complex.

Acknowledgments

We acknowledge the Ohio Supercomputing Center for providing computational resources. We gratefully acknowledge financial support for this work provided by the Department of Energy, Office of Basic Energy Sciences and Catalysis Science Division through Grant DE-FG02-03ER15478.

References

[1] F. Gao, S.M. McClure, Y. Cai, K.K. Gath, Y. Wang, M.S. Chen, Q.L. Guo, D.W. Goodman, Surf. Sci. 603 (2009) 65.
[2] R. van Rijn, O. Balmes, A. Resta, D. Wermeille, R. Westerstrom, J. Gustafson, R. Felici, E. Lundgren, J.W.M. Frenken, Phys. Chem. Chem. Phys. 13 (2011) 13167.
[3] B.L.M. Hendriksen, J.W.M. Frenken, Phys. Rev. Lett. 89 (2002) 046101.
[4] J. Gustafson, R. Westerstroem, A. Mikkelsen, X. Torrelles, O. Balmes, N. Bovet, J.N. Andersen, C.J. Baddeley, E. Lundgren, Phys. Rev. B 78 (2008) 045423.
[5] H. Over, Chem. Rev. 112 (2012) 3356.
[6] J.F. Weaver, Chem. Rev. 113 (2013) 4164.
[7] J. Bergeld, B. Kasemo, D.V. Chakarov, Surf. Sci. 495 (2001) L815.
[8] R.A. Ojifinni, N.S. Froemming, J. Gong, M. Pan, T.S. Kim, J.M. White, G. Henkelman, C.B. Mullins, J. Am. Chem. Soc. 130 (2008) 6801.
[9] S.D. Ebbesen, B.L. Mojet, L. Lefferts, Phys. Chem. Chem. Phys. 11 (2009) 641.
[10] J.L. Gong, R.A. Ojifinni, T.S. Kim, J.D. Stiehl, S.M. McClure, J.M. White, C.B. Mullins, Top. Catal. 44 (2007) 57.
[11] X.Q. Gong, P. Hu, R. Raval, J. Chem. Phys. 119 (2003) 6324.
[12] H.F. Wang, R. Kavanagh, Y.L. Guo, Y. Guo, G.Z. Lu, P. Hu, Angew. Chem. Int. Ed. 51 (2012) 6657.
[13] G.Y. Wang, W.X. Zhang, Y.C. Cui, H.L. Lian, D.Z. Jiang, T.H. Wu, Chin. J. Catal. 22 (2001) 408.
[14] H.B. Zou, X.F. Dong, W.M. Lin, Appl. Surf. Sci. 253 (2006) 2893.
[15] K. Sirichalprasert, A. Luengnaruemitchai, S. Pongstabodee, Int. J. Hydrog. Energy 32 (2007) 915.
[16] D. Gamarra, A. Martinez-Arias, J. Catal. 263 (2009) 189.
[17] X.W. Xie, Y. Li, Z.Q. Liu, M. Haruta, W.J. Shen, Nature 458 (2009) 746.
[18] S.H. Oh, G.B. Hoflund, J. Catal. 245 (2007) 35.
[19] H.H. Kan, R.J. Colmyer, A. Asthagiri, J.F. Weaver, J. Phys. Chem. C 113 (2009) 1495.
[20] F. Zhang, T. Li, L. Pan, A. Asthagiri, J.F. Weaver, Catal. Sci. Technol. 4 (2014) 3826.
[21] F. Zhang, L. Pan, T. Li, J. Diulus, A. Asthagiri, J.F. Weaver, J. Phys. Chem. C 118 (2014) 28647.
[22] J.F. Weaver, F. Zhang, L. Pan, T. Li, A. Asthagiri, Acc. Chem. Res. 48 (2015) 1515.
[23] N.M. Martin, M. Van den Bossche, H. Gronbeck, C. Hakanoglu, F. Zhang, T. Li, J. Gustafson, J.F. Weaver, E. Lundgren, J. Phys. Chem. C 118 (2014) 1118.
[24] H.H. Kan, R.B. Shumbera, J.F. Weaver, Surf. Sci. 602 (2008) 1337.
[25] H.H. Kan, J.F. Weaver, Surf. Sci. 603 (2009) 2671.
[26] H.H. Kan, J.F. Weaver, Surf. Sci. 602 (2008) L53.
[27] C. Hakanoglu, F. Zhang, A. Antony, A. Asthagiri, J.F. Weaver, Phys. Chem. Chem. Phys. 15 (2013) 12075.
[28] H. Conrad, G. Ertl, J. Kuppers, Surf. Sci. 76 (1978) 323.
[29] G. Kresse, J. Hafner, J. Non-Cryst. Solids 156 (1993) 956.
[30] G. Kresse, J. Non-Cryst. Solids 193 (1995) 222.
[31] P.E. Blochl, Phys. Rev. B 50 (1994) 17953.
[32] J.P. Perdew, K. Burke, M. Ernzerhof, Phys. Rev. Lett. 77 (1996) 3865.
[33] C. Hakanoglu, J.M. Hawkins, A. Asthagiri, J.F. Weaver, J. Phys. Chem. C 114 (2010) 11485.
[34] J.F. Weaver, C. Hakanoglu, A. Antony, A. Asthagiri, J. Am. Chem. Soc. 133 (2011) 16196.
[35] A. Antony, A. Asthagiri, J.F. Weaver, Phys. Chem. Chem. Phys. 14 (2012) 12202.
[36] G. Henkelman, B.P. Uberuaga, H. Jonsson, J. Chem. Phys. 113 (2000) 9901.

Please cite this article as: J. Choi, et al., Surf. Sci. (2015), http://dx.doi.org/10.1016/j.susc.2015.08.043